Research Article

Savas Evran*

Mathematical analysis of nanoparticle type and volume fraction on heat transfer efficiency of nanofluids

https://doi.org/10.1515/phys-2025-0158
received December 18, 2024; accepted May 07, 2025

Abstract: Nanofluids (NFs) have been implemented in several areas to increase heat transfer efficiency. Thus, efficiency for heat energy can be achieved. In this study, the effect of nanoparticle (NP) type, volume fraction, and Re number on the heat transfer efficiency of NFs were analyzed numerically, statistically, and theoretically. Heat transfer coefficient, number of transfer units, wall shear stress, and friction factor were selected as the heat transfer efficiency of NFs. ANSYS Fluent software was utilized to carry out computational fluid dynamics analyses. The numerical calculation scheme was implemented by employing the Taguchi L9 orthogonal array with three decisive factors. NP type, volume fraction, and Re number were assumed as decisive factors with three levels. Signal-to-noise ratio analysis was utilized to determine the direction of impact and ideal levels of each decisive factor on the heat transfer efficiency of NFs. Significance levels and contribution rates of the decisive factors on the heat transfer efficiency were calculated with Analysis of Variance. According to the mathematical responses, the most effective NPs on h and τ_w were identified as Gr, Al_2O_3, and Cu, respectively, whereas the most effective NPs on number of transfer units are found to be Cu, Al_2O_3, and Gr, respectively. In addition, the increase in Re number from 6,000 to 8,000 causes an increase in h and τ_w and a decrease in NTU and f. The data achieved from the mathematical research may be utilized to be a guide paper in experimental analyses.

Keywords: ANOVA, fluid dynamics, heat transfer efficiency, nanoparticle type, Taguchi approach

*** Corresponding author: Savas Evran**, Faculty of Applied Sciences, Department of Jewelry and Jewelry Design, Marmara University, 34865, Istanbul, Turkey, e-mail: sevran@marmara.edu.tr

Nomenclature

A_c	cross-sectional area of tube at inlet
ANOVA	analysis of variance
A_{sr}	tube surface area
$C_{1\epsilon}$, C_2, $C_{3\epsilon}$, C_μ	constants
$C_{p,nf}$	specific heat of NFs
c_p	specific heat
D_{Tube}	diameter of tube
E	energy
$\vec{F}$	external body forces
f	friction factor
G_k	emergence of turbulence kinetic energy because of the mean velocity gradients
G_b	emergence of turbulence kinetic energy because of buoyancy
g	gravity
HTE	heat transfer efficiency
h	heat transfer coefficient
k_{nf}	thermal conductivity of NF
k_{bf}	thermal conductivity based on base fluid
k	turbulence kinetic energy
k	thermal conductivity of the fluid
$\bar{M}_i$	average HTE value at optimum levels for particle
$\dot{m}$	mass flow rate of fluid
NFs	nanofluids
NP	nanoparticle
NTU	number of transfer units
$\overline{Nu}_D$	Nusselt's number
Pr	Prandtl numbers
$\dot{Q}$	rate of heat transfer
$\overline{Re}_i$	average HTE value at optimum levels for Re number
Re	Reynolds number
$\vec{r}$	location vector for the field point
$\vec{r}_w$	combination of all relevant wall boundaries
S_k, S_ϵ	source terms specified by the user

S/N	signal-to-noise
S_m	mass added to the continuous phase from the dispersed second phase
T_e, T_i	exit and inlet temperature of fluid
$T_{f,ave}$	average fluid temperature
TI	turbulence intensity
$\bar{T}_{OM}$	overall mean
T_s	average temperature of wall surface
t	time
$\overline{VF}_i$	average HTE value at optimum levels for volume fraction
$\mathbb{v}$	fluid velocity
Y_M	impact of the fluctuating dilatation for compressible turbulence to the mean dissipation rate
y	normal remoteness from the wall at cell centers
μ	viscosity of the fluid
μ_t	Eddy viscosity
σ_k	turbulent Prandtl numbers according to k
σ_ϵ	turbulent Prandtl numbers according to ϵ
ρ	fluid density
$\rho\vec{\mathbb{v}}$	gravitational body force
Γ	blending function
ϵ	rate of dissipation
τ_w	wall shear stress
φ	volume fraction
ρ_{nf}	density of NF
ρ_{bf}	density for base fluid
μ_{nf}	viscosity of NFs
μ_{bf}	viscosity of base fluid
$\bar{\mu}_{HTE}$	optimal heat transfer efficiency

1 Introduction

Nanofluids (NFs) obtained with nanoparticles (NPs) and base fluids were utilized to increase the heat transmission of the fluid [1,2]. NFs were produced by combining NPs with high thermal conductivity and a working liquid with low thermal conductivity [3]. NPs with high thermal conductivity increase the heat transfer coefficient of NFs [2]. NPs may be grouped under three headings such as metallic, oxide, and carbon [4]. Since each NP has various mechanical, physical, and thermal properties, it can also affect the properties of NFs. Due to these properties of NFs, it may of great potential use in various sectors [5]. Many studies have been reported about various NPs such as Al_2O_3 [6], TiO_2 [7], Cu [8], CuO [9], Cu_2O [10], MgO [11], carbon nanotubes [12], multi-wall carbon nanotubes [13], single-walled carbon nanotube [14], ZrO_2 [15], SiO_2 [16], Si_3N_4 [3], SiC [17], GO [18], F_3O_4 [19], Ag [20], Ni [21], SnO_2 [22], BN [23], AIN [24], ZnO [25], CB [26], CeO_2 [27]. Due to the large number of NPs, NFs have been produced for use in different areas such as nuclear power plant [28], solar energy systems [29], biomedicine [30], heat exchangers [31], jet impingement [32], lubrication machining [33], automotive application [34], electronic cooling systems [35], *etc.* In addition, different fluids such as water [36], nitride-water [37], engine oil [38], and ethylene glycol [39] have been used as base fluids. Thus, using different base fluids and NPs provide improvements in the thermophysical characteristics of the NFs. Various research works on NFs have been conducted by many scientists in the literature. Among the studies, heat exchangers are particularly prevalent. Calviño *et al.* [15] stated the heat transfer efficiency of ZrO_2 NF using heat exchangers and used four various volume fractions of NPs. Laminar and turbulent flow were chosen for flow. As a result of their study, they found that ZrO_2 can have potential effect for heat exchangers. Zhang *et al.* [40] evaluated the influence of Cu NF in heat exchangers and detected that the increase in Re number and volume fractions of NPs also increased the heat transfer coefficient. Also, they detected that the rise in Re number provides a rise on pressure difference. Fares *et al.* [41] examined that graphene nanofluids (GNF) NFs on heat exchangers stated a 29% increase in heat transfer coefficient and a 19% increase in average thermal efficiency. They also found that GNF NF has an enhancing impact on thermal characteristic. Fule *et al.* [42] improved the heat transfer coefficient of heat exchangers by employing CuO NF and observed a 37.3% improvement compared to working fluid, using 0.1% NPs. Said *et al.* [43] examined CuO NFs using a heat exchanger. They found that NF developed the average heat transfer coefficient by 7% and convective heat transfer by 11.39%. Salameh *et al.* [44] analyzed the impact of various volume fractions of NPs using NFs including CuO, Al_2O_3, and T_iO_2 in heat exchangers. They determined that NFs ensure upper heat transfer coefficient than base fluids. The authors also found that CuO NFs demonstrated the highest performance. Qi *et al.* [45] determined the impact of TiO_2 NF on thermal efficiency and pressure change in heat exchangers and stated that the increase in the volume fraction values of NPs also caused an increase in the heat transfer rate. They observed that NFs exhibited better thermal effectiveness compared to base liquids. Ajeeb *et al.* [46] stated the heat transfer efficiency using Al_2O_3 NF in heat exchangers and reached an improvement of 9.1% for Al_2O_3 in the thermal conductivity. Zheng *et al.* [47] carried out heat transfer improvement analysis utilizing various NFs in heat exchangers and stated that the most suitable concentration for thermal improvement utilizing CuO NF was 0.5% by weight. Bahiraei and Ahmadi [48] numerically carried out thermohydraulic

performance analyses in heat exchangers using alumina-water NFs. They stated that the increase in Re number and concentration play major role on the convective heat transfer and general heat transfer coefficients. In addition to these studies, many studies [49–52] involving NFs and different methods have been conducted. As can be seen from the mentioned literature summary, there are a lot of studies involving computational fluid dynamics (CFD) approaches. Some of these studies have been confirmed experimentally. However, studies containing statistical and theoretical validations are limited in number. In this study, the impacts of NP type, Volume fraction (VF), and Re number in the heat transfer coefficient, number of transfer units, wall shear stress, and friction factor of NFs were analyzed numerically, statistically, and theoretically.

2 Materials

In the numerical, theoretical, and statistical analyses, three different NPs were chosen to create NFs. Each NP has various properties. Thus, the impact of each NP property in the NFs was also determined. The water in the model was determined as base fluid. The properties such as density, specific heat, thermal conductivity, and viscosity of base fluid (water) were used as 998.2 kg/m^3, 4,182 J/kg K, 0.6 W/m K, and 0.001003 kg/m s, respectively [53]. The properties for the NPs utilized are listed in Table 1 [54].

To analyze the properties of NFs, different volume factions of NPs and base fluid were used. Volume fraction is determined as follows [55]:

$$\varphi = \frac{V_{\mathrm{np}}}{V_{\mathrm{bf}} + V_{\mathrm{np}}}. \tag{1}$$

Density of NFs is solved as follows [56]:

$$\rho_{\mathrm{nf}} = \rho_{\mathrm{bf}}(1 - \varphi) + \rho_{\mathrm{np}}\varphi. \tag{2}$$

The specific heat capacities of NFs may be considered as follows [57]:

$$C_{\mathrm{p,nf}} = \frac{(1 - \varphi)_{\rho\mathrm{bf}} C_{\mathrm{p,bf}} + \varphi_{\rho\mathrm{np}} C_{\mathrm{p,np}}}{\rho_{\mathrm{nf}}}. \tag{3}$$

The thermal conductivity of NF depending on working fluid is examined as follows [58,59]:

Table 1: Properties of NPs [54]

Properties	Symbol	Unit	Gr	Al_2O_3	Cu
Density	ρ	kg m^{-3}	2,200	3,700	8,933
Specific heat	C_p	J/kg °C^{-1}	790	880	385
Thermal conductivity	k	W/mK	5,000	46	401

$$\frac{k_{\mathrm{nf}}}{k_{\mathrm{bf}}} = \frac{(k_{\mathrm{np}} + 2k_{\mathrm{bf}}) - 2\varphi(k_{\mathrm{bf}} - k_{\mathrm{np}})}{(k_{\mathrm{np}} + 2k_{\mathrm{bf}}) + \varphi(k_{\mathrm{bf}} - k_{\mathrm{np}})}. \tag{4}$$

The effective viscosity of NFs can be calculated as follows [60]:

$$\mu_{\mathrm{nf}} = \mu_{\mathrm{bf}} \frac{1}{(1 - \varphi)^{2.5}}. \tag{5}$$

Properties of NFs in accordance with Eqs. (1)–(5) are defined in Table 2.

As described in Table 2, the increase in the VFs of the NPs provides an increase in the effective density, thermal conductivity, and viscosity of the NFs. However it leads to a decrease in effective specific heat.

3 Numerical analysis

ANSYS Fluent software was utilized for CFD analysis of the heat transfer efficiency of NFs. CFD approach was used for numerical calculations. A tube of 1,000 mm length and 16 mm diameter was used in modeling. The heat flux of 3,500 W/m^{2}K was applied to the tube. In mesh analyses, MultiZone method with uniform surface mesh, Haxa mapped mesh, and free mesh types was selected. In addition, edge sizing, inflation, and face meshing were utilized to perform precise analysis. Absolute criteria for residuals base on continuity, velocity for x, y, z, energy, k, epsilon was selected as 10^6. Hybrid model was applied as solution initialization. Coupled scheme in solution methods was chosen. For precise analyses, turbulence intensity values were calculated for each Re number. Turbulence intensity may be considered [61]:

$$\mathrm{T.I} = 0.16\,\mathrm{Re}^{-0.125}. \tag{6}$$

Table 2: Properties of NFs

NFs	ρ (kg m^{-3})	C_p (J kg °C^{-1})	k (W m^{-1} °C^{-1})	μ (kg/m-s)
0.5% Gr	1004.209	4144.844	0.609042	0.001016
1.0% Gr	1010.218	4108.131	0.618175	0.001029
1.5% Gr	1016.227	4071.851	0.627401	0.001042
0.5% Al_2O_3	1011.709	4121.620	0.608699	0.001016
1.0% Al_2O_3	1025.218	4062.831	0.617482	0.001029
1.5% Al_2O_3	1038.727	4005.572	0.626351	0.001042
0.5% Cu	1037.874	4018.596	0.609005	0.001016
1.0% Cu	1077.548	3867.224	0.618100	0.001029
1.5% Cu	1117.222	3726.603	0.627287	0.001042

The formulas such as continuity, momentum, stress tensor, and energy in finite element software ANSYS Fluent may be determined, respectively as follows [62]:

$$\frac{\partial \rho}{\partial t} + \nabla(\rho \vec{v}) = S_{\mathrm{m}}, \tag{7}$$

$$\frac{\partial}{\partial t}(\rho \vec{v}) + \nabla(\rho \vec{v}\vec{v}) = -\nabla p + \nabla \bar{\bar{\tau}} + \rho \vec{g} + \vec{F}, \tag{8}$$

$$\bar{\bar{\tau}} = \mu\left[(\nabla \vec{v} + \nabla \vec{v}^{\mathrm{T}}) - \frac{2}{3}\nabla \vec{v} I\right], \tag{9}$$

$$\frac{\partial(\rho E)}{\partial t} + \nabla\cdot[\vec{v}(\rho E + p)] = \nabla\cdot\left(k_{\mathrm{eff}}\nabla T - \sum_j h_j \vec{J_j} + (\bar{\bar{\tau}}_{\mathrm{eff}}\cdot\vec{v})\right) + S_{\mathrm{h}}. \tag{10}$$

The k-epsilon realizable and near wall treatment in the viscos model was selected. The considered transport approach for k and ε can be described as follows [62]:

$$\frac{\partial}{\partial t}(\rho \mathrm{k}) + \frac{\partial}{\partial x_j}(\rho \mathrm{k} u_j) = \frac{\partial}{\partial x_j}\left[\left(\mu + \frac{\mu_{\mathrm{t}}}{\sigma_{\mathrm{k}}}\right)\frac{\partial k}{\partial x_j}\right] + G_{\mathrm{k}} + G_{\mathrm{b}} - \rho\epsilon - Y_{\mathrm{M}} + S_{\mathrm{k}}, \tag{11}$$

$$\frac{\partial}{\partial t}(\rho \epsilon) + \frac{\partial}{\partial x_j}(\rho \epsilon u_j) = \frac{\partial}{\partial x_j}\left[\left(\mu + \frac{\mu_t}{\sigma_\epsilon}\right)\frac{\partial \epsilon}{\partial x_j}\right] + \rho C_1 S_\epsilon - \rho C_2 \frac{\epsilon^2}{k + \sqrt{\upsilon\epsilon}} + C_{1\epsilon}\frac{\epsilon}{k}C_{3\epsilon}G_{\mathrm{b}} + S_\epsilon. \tag{12}$$

The eddy viscosity can be solved as follows [62]:

$$\mu_{\mathrm{t}} = \rho C_\mu \frac{k^2}{\epsilon}. \tag{13}$$

The model constants in k-epsilon model can be solved as follows [62]:

$$C_{1\epsilon} = 1.44, \quad C_2 = 1.9, \quad \sigma_{\mathrm{k}} = 1.0, \quad \sigma_\epsilon = 1.2. \tag{14}$$

Two layer model depending on the enhanced wall treatment can be defined as follows [62]:

$$\mathrm{Re}_{\mathrm{y}} \equiv \frac{\rho y\sqrt{k}}{\mu}, \tag{15}$$

$$y \equiv \min_{\vec{r}_{\mathrm{w}} \epsilon \Gamma_{\mathrm{w}}} \vec{r} - \vec{r}_{\mathrm{w}}, \tag{16}$$

$$\mu_{\mathrm{t,2layer}} = \rho C_{\mathrm{m}} l_{\mathrm{m}} \sqrt{k}, \tag{17}$$

$$l_{\mathrm{m}} = y C_{\mathrm{l}}^{*}(1 - e^{-\mathrm{Re}_{\mathrm{y}}/A_\mu}), \tag{18}$$

$$\mu_{\mathrm{t,enh}} = \lambda_\epsilon \mu_{\mathrm{t}}(1 - \lambda_\epsilon)\mu_{\mathrm{t,2\,layer}}. \tag{19}$$

Enhanced wall functions can be determined as follows [62]:

$$u^{+} = e^{\Gamma} u^{+}_{\mathrm{lam}} + e^{\frac{1}{\Gamma}} u^{+}_{\mathrm{turb}}, \tag{20}$$

$$\Gamma = -\frac{0.01(y^{+})^4}{1 + 5y^{+}}, \tag{21}$$

$$\frac{\mathrm{d}u^{+}}{\mathrm{d}y^{+}} = e^{\Gamma}\frac{\mathrm{d}u^{+}_{\mathrm{lam}}}{\mathrm{d}y^{+}} + e^{\frac{1}{\Gamma}}\frac{\mathrm{d}u^{+}_{\mathrm{turb}}}{\mathrm{d}y^{+}}. \tag{22}$$

To calculate the heat transfer efficiency of NFs accurately, two-layer model depending on the improved wall treatment was applied. Thus, it was aimed to obtain high precision results in CFD analyses.

4 Statistical analysis

Statistical methods such as Taguchi method and variance analysis were considered to evaluate the impact of decisive factor for various levels on the heat transfer efficiency of the NFs. Nine CFD analyses were performed using different levels of decisive factors such as NP, VF, and Re number. The combination of NP, VF, and Re number according to different levels was determined in accordance with Taguchi L9 orthogonal array with three levels. Decisive factors and different levels are presented in Table 3.

As described in Table 3, the levels of NPs are determined as Gr, Al_2O_3, and Cu, respectively. VFs of NPs were chosen as 0.5, 1.0, and 1.5%. To decide the effect of the Re number, three different values were selected and considered as 6,000, 7,000, and 8,000, respectively. Signal-to-noise (S/N) ratio analysis was utilized to explain the influence of each decisive factor on the heat transfer efficiency depending on different levels. The results obtained from the CFD data in this analysis were adapted to S/N ratios. Two different characteristics such as “the Larger is Better” and “the Smaller is Better” were utilized in the calculation of S/N ratios. Thus, it was aimed to obtain the highest h, number of transfer units (NTU), and T_{w} values and the lowest f values for NFs. For the maximum h, NTU, and T_{w} values, “the Larger is Better” characteristic was assumed and, “the Smaller is Better” characteristic was considered for the minimum f value. “The Larger is Better” and “the Smaller is Better” characteristics are explained in Eqs. (23) and (24), respectively [63]:

Table 3: Decisive factors at different levels

Decisive factors	Symbol	Level 1	Level 2	Level 3
Material	M	Gr	Al_2O_3	Cu
Volume fraction	VF	0.5%	1.0%	1.5%
Re number	Re	6,000	7,000	8,000

$$(S/N)_{LB} \text{ for } h, \text{ NTU, } \tau w = -10.\log\left(n^{-1}\sum_{i=1}^{n}(y_i^2)^{-1}\right), \quad (23)$$

$$(S/N)_{SB} \text{ for } f = -10.\log\left(n^{-1}\sum_{i=1}^{n}(y_i)^2\right). \quad (24)$$

Minitab R15 program was used for statistical calculation of each characteristic and creation of graphs depending on S/N ratios.

5 Heat transfer efficiency calculation

In mathematical analyses, h, NTU, τ_w, and f were chosen as the heat transfer efficiency of NFs. The NFs were passed through a tube exposed to heat flux. The heat flux was kept constant but the levels of NP type, VF, and Re number were changed in each analysis. Thus, h, NTU, τ_w, and f values were calculated under constant heat flux.

h for tube can be defined as follows [64]:

$$h = \frac{\dot{Q}}{A_{sr}(T_s - T_{f,ave})}. \quad (25)$$

$\dot{Q}$ obtained by using working fluid in tube may be evaluated as follows [64]:

$$\dot{Q} = \dot{m}c_p(T_e - T_i), \quad (26)$$

$\dot{m}$ for working fluid may be defined as follows [64]:

$$\dot{m} = \rho v A_c. \quad (27)$$

NTU for tube can be calculated as follows [64]:

$$NTU = \frac{hA_{sr}}{\dot{m}c_p}. \quad (28)$$

τ_w for tube can be solved as follows [61]:

$$\tau_w = \frac{f\rho v^2}{8}. \quad (29)$$

Re number can be defined as follows [64]:

$$Re = \frac{\rho v D}{\mu}. \quad (30)$$

6 Results and discussion

The main goal of the research is to observe the impact of NP, VF, and Re number on the heat transfer efficiency of NFs numerically, statistically, and theoretically. Numerical analyses for the heat transfer efficiency were carried out with CFD approach and the numerical data are listed in Table 4.

As can be understood from Table 4, the average values obtained for h, NTU, τ_w, and f depending on the L9 orthogonal array are 2266.9 W/m^{2}K, 0.3146, 0.8430 Pa, and 0.0343, respectively. The S/N ratios of the CFD results in Table 4 are tabulated in Table 5.

S/N ratios for h, NTU, and τ_w were calculated according to "Larger is Better" quality characteristic and for f was solved in accordance with "Smaller is Better" quality characteristic.

6.1 Selection of optimum levels

In this study, it was aimed to obtain maximum h, NTU, and τ_w and minimum f values. The optimum levels of NP, VF, and Re number on the heat transfer efficiency of NFs were calculated utilizing average S/N ratios and CFD data corresponding to each level of each decisive factor. Overall S/N ratios and CFD results are stated in Tables 6 and 7, respectively.

As described from response table for h and NTU, the optimum h were considered as the first level for NP and the third levels for VF and Re number. For NTU, it was calculated as the third levels of NP and VF and the first level of Re number.

From response table for τ_w and f, the optimum τ_w were obtained using the first level of NP, the third level of VF, and the third level of Re number. It was determined that the third level of the Re number and all levels of NP and VF can be used to calculate the optimum f value. Main effect plots were drawn using average S/N ratios in Tables 6 and 7

Table 4: CFD data depending on L9 orthogonal array

Test	Decisive factors			CFD data			
	M	VF	Re	h, (W/m^{2}K)	NTU, (−)	τ_w, (Pa)	f, (−)
1	Gr	0.5%	6,000	1994.3	0.3158	0.6474	0.0359
2	Gr	1.0%	7,000	2289.7	0.3097	0.8567	0.0342
3	Gr	1.5%	8,000	2586.4	0.3049	1.0966	0.0329
4	Al_2O_3	0.5%	7,000	2260.0	0.3085	0.8341	0.0342
5	Al_2O_3	1.0%	8,000	2546.6	0.3047	1.0598	0.0329
6	Al_2O_3	1.5%	6,000	2021.4	0.3230	0.6583	0.0359
7	Cu	0.5%	8,000	2502.0	0.3065	1.0209	0.0329
8	Cu	1.0%	6,000	1967.9	0.3298	0.6188	0.0359
9	Cu	1.5%	7,000	2233.7	0.3288	0.7945	0.0342
Overall mean values				2266.9	0.3146	0.8430	0.0343

Table 5: S/N ratios for heat transfer efficiency

Test	Decisive factors			S/N ratios (η), dB			
	M	VF	Re	η for h	η for NTU	η for τ_w	η for f
1	Gr	0.5%	6,000	65.9958	−10.0110	−3.7765	28.9092
2	Gr	1.0%	7,000	67.1956	−10.1823	−1.3439	29.3215
3	Gr	1.5%	8,000	68.2539	−10.3167	0.8010	29.6646
4	Al_2O_3	0.5%	7,000	67.0822	−10.2148	−1.5754	29.3214
5	Al_2O_3	1.0%	8,000	68.1192	−10.3222	0.5045	29.6647
6	Al_2O_3	1.5%	6,000	66.1130	−9.8163	−3.6314	28.9092
7	Cu	0.5%	8,000	67.9657	−10.2712	0.1797	29.6642
8	Cu	1.0%	6,000	65.8801	−9.6340	−4.1697	28.9089
9	Cu	1.5%	7,000	66.9805	−9.6607	−1.9981	29.3211

Table 6: Response table for h and NTU

Level	h (W/m^2 K)						NTU (−)					
	S/N ratios			Mean values			S/N ratios			Mean values		
	M	VF	Re	M	VF	Re	M	VF	Re	M	VF	Re
1	67.15	67.01	66.00	2290	2252	1995	−10.170	−10.166	−9.820	0.3101	0.3103	0.3229
2	67.10	67.06	67.09	2276	2268	2261	−10.118	−10.046	−10.019	0.3121	0.3147	0.3157
3	66.94	67.12	68.11	2235	2281	2545	−9.855	−9.931	−10.303	0.3217	0.3189	0.3054
Delta	0.21	0.10	2.12	56	28	550	0.315	0.234	0.483	0.0116	0.0086	0.0175
Rank	2	3	1	2	3	1	2	3	1	2	3	1

to define the influence of each decisive factor on the h, NTU, τ_w, and f depending on the different levels. Main effect plots for h and NTU are presented in Figures 1 and 2.

Figure 1 shows that the most influential NPs on h were identified as Gr, Al_2O_3, and Cu, respectively. Increase in the VF of NPs from 0.5 to 1.5% causes an increase in h. This finding was identified by a study by Garud and Lee [65]. In addition, increasing the Re number from 6,000 to 8,000 provides an increase in h. This finding is supported by a previous study [65] and it is stated that increasing Re number also increases h value. As seen in Figure 2, the most effective NPs on NTU were evaluated as Cu, Al_2O_3, Gr, respectively. An increase in the VF values of NPs from 0.5 to 1.5% causes an increase in NTU, whereas the increase in Re number from 6,000 to 8,000 causes a decrease for NTU. Main effect plots for τ_w and f are displayed in Figures 3 and 4.

As described from Figure 3, the most dominant NPs on τ_w were determined as Gr, Al_2O_3, and Cu, respectively. Increase in the VF of NPs from 0.5 to 1.5% and Re number from 6,000 to 8,000 causes an increase in τ_w. As explained from Figure 4, it was found that NP and VFs did not have

Table 7: Response table for τ_w and f

Level	τ_w (Pa)						f (−)					
	S/N ratios			Mean values			S/N ratios			Mean values		
	M	VF	Re	M	VF	Re	M	VF	Re	M	VF	Re
1	−1.440	−1.724	−3.859	0.8669	0.8341	0.6415	29.3	29.3	28.91	0.0343	0.0343	0.0359
2	−1.567	−1.670	−1.639	0.8507	0.8451	0.8284	29.3	29.3	29.32	0.0343	0.0343	0.0342
3	−1.996	−1.610	0.495	0.8114	0.8498	1.0591	29.3	29.3	29.66	0.0343	0.0343	0.0329
Delta	0.556	0.115	4.354	0.0555	0.0157	0.4176	0	0	0.76	0	0	0.0030
Rank	2	3	1	2	3	1	2.5	2.5	1	2.5	2.5	1

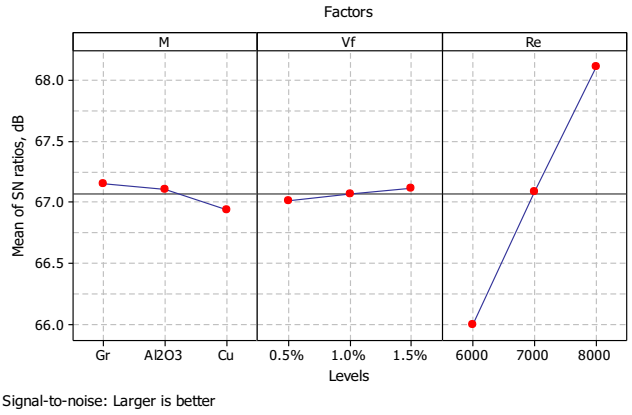

Figure 1: Effects of M, VF, and Re on *h*.

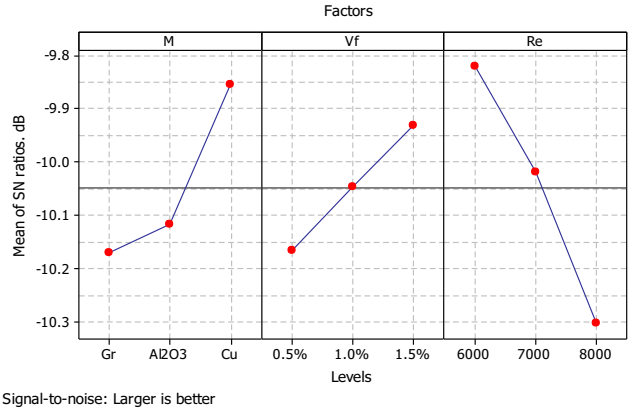

Figure 2: Effects of M, VF, and Re on NTU.

any effect on *f*. This finding can be explained by Eq. (35). According to the Colebrook equation [64], *f* depends on the relative roughness and Re number. However, increasing the Re number from 6,000 to 8,000 provides a decrease in the *f* value. A finding is supported by a study and it is stated that an increase in the Re number from 6,000 to 8,000 decreases the *f* value [65].

6.2 Analysis of variance

ANOVA was implemented according to general approach at 95% confidence interval to decide the percentage contributions and importance levels of NP, VF, and Re number on the *h*, NTU, τ_w, and *f*. ANOVA data depending on *h* and NTU are presented in Table 8.

According to the *F* test results for 95% confidence interval in ANOVA, although Re number on h and NTU were determined as significant decisive factors, NP and VF were determined as insignificant parameters. The most effective decisive factors on h were obtained as Re number with 98.58% impact, NP with 1.09% impact, and VF with 0.26% impact, respectively. For NTU, the most powerful decisive factors were decided as Re number with 56.30% impact, NP with 28.04% impact, and VF with 13.54% impact, respectively. ANOVA data for τ_w and *f* are given in Table 9.

According to ANOVA data for τ_w and *f*, although the most significant decisive factor on τ_w was selected as Re number due to 95% confidence level, NP and VF were determined as insignificant decisive factors. The most dominant decisive factors on τ_w were obtained as Re number with 97.88% impact, NP with 1.82% impact, and VF with 0.14% impact, respectively.

7 Statistical validation

The average values obtained from the CFD results corresponding to each level of each decisive factor were used to

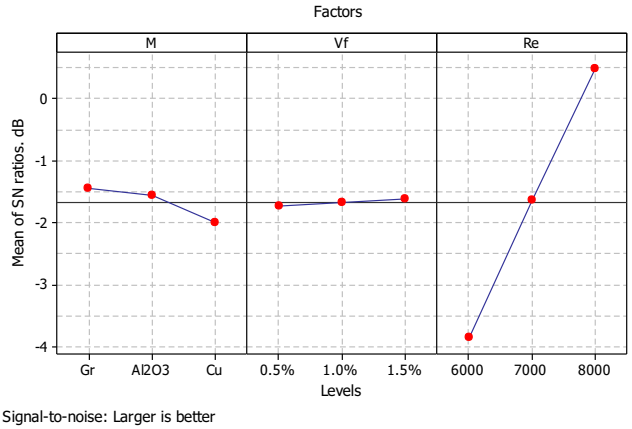

Figure 3: Effects of M, VF, and Re on τ_w.

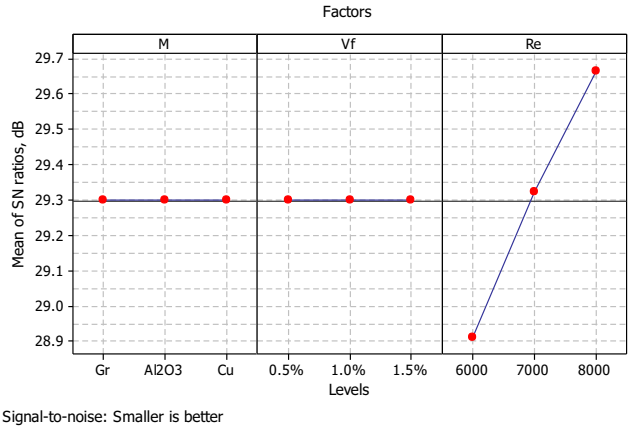

Figure 4: Effects of M, VF, and Re on *f*.

Table 8: ANOVA results for h and NTU

Source	h						NTU				
	DF	Seq SS	Adj MS	F	P	% Impact	Seq SS	Adj MS	F	P	% Impact
M	2	5,011	2,505	14.74	0.064	1.09	0.000231	0.00012	13.15	0.071	28.04
VF	2	1,216	608	3.58	0.218	0.26	0.000112	0.00006	6.35	0.136	13.54
Re	2	454,669	227,335	1337.36	0.001	98.58	0.000465	0.00023	26.4	0.036	56.30
Error	2	340	170			0.07	0.000018	0.00001			2.13
Total	8	461,236				100	0.000825				100
R-Sq = 99.93% and R-Sq(adj) = 99.71%							R-Sq = 97.87% and R-Sq(adj) = 91.47%				

Table 9: ANOVA results for τ_w and f

Source	τ_w						f				
	DF	Seq SS	Adj MS	F	P	% Impact	Seq SS	Adj MS	F	P	% Impact
M	2	0.00489	0.002445	12.11	0.076	1.82	0	0	**	**	0
VF	2	0.000387	0.000194	0.96	0.511	0.14	0	0	**	**	0
Re	2	0.262558	0.131279	650.23	0.002	97.88	0.0000134	0.0000067	**	**	100
Error	2	0.000404	0.000202			0.15	0	0			0
Total	8	0.268239				100	0.0000134				100
R-Sq = 99.85% and R-Sq(adj) = 99.40%							R-Sq = 100.00% and R-Sq(adj) = 100.00%				

perform statistical verification of the heat transfer efficiency. These values are given in Tables 6 and 7. The optimum values of h, NTU, and τ_w was calculated by employing the optimum levels of important decisive factors. The estimated mean of h, NTU, and τ_w can be evaluated as follows [63]:

$$\bar{\mu}_{HTE} = \bar{M}_i + \overline{VF}_i + \overline{Re}_i - 2\bar{T}_{OM}. \quad (31)$$

$\bar{T}_{OM}$ represents the overall mean of nine CFD analyses based on the L9 orthogonal array. $\bar{T}_{OM}$ for h, NTU, τ_w, and f were calculated as 2266.9 W/m^{2}K, 0.3146, 0.8430 Pa, and 0.0343, respectively. $\bar{M}_i$ denotes the overall data of heat transfer efficiency at the optimum level of NPs. $\bar{M}_i$ for h, NTU, τ_w, and f were found as 2,290, 0.3217, 0.8669, and 0.0343, respectively. $\overline{VF}_i$ expresses the overall data of heat transfer efficiency at the optimum level of VF. $\overline{VF}_i$ for h, NTU, τ_w, and f were evaluated as 2,281, 0.3189, 0.8498, and 0.0343, respectively. $\overline{Re}_i$ means the overall data of heat transfer efficiency depending on the optimum level of Re number. $\overline{Re}_i$ for h, NTU, τ_w, and f were evaluated as 2,545, 0.3229, 1.0591, and 0.0329, respectively. Substituting the data of different terms in Eq. (31), estimated heat transfer

Table 10: Comparison of CFD and predict Taguchi data

Results	h for $M_1VF_3Re_3$	NTU for $M_3VF_3Re_1$	τ_w for $M_1VF_3Re_3$	f for $M_{all}VF_{all}Re_3$
CFD result	2586.4 W/m^2 K	0.3377	1.0966 Pa	0.0329
Taguchi result	2582.2 W/m^2 K	0.3343	1.0898 Pa	0.0329
Difference	0.2%	1%	0.6%	0%

Table 11: Comparison of CFD and theoretical results

Results	h for $M_1VF_3Re_3$	NTU for $M_3VF_3Re_1$	τ_w for $M_1VF_3Re_3$	f for $M_{all}VF_{all}Re_3$
CFD result	2586.4 W/m^{2}K	0.3377	1.0966 Pa	0.0329
Theoretical result	2568.1 W/m^{2}K	0.3381	1.0943 Pa	0.0328
% Difference	0.7%	0.1%	0.2%	0.3%

efficiency was obtained. The comparison of the CFD and predict Taguchi results obtained is presented in Table 10.

Table 10 displays that the differences for h, NTU, τ_w, and f are 0.2, 1, 0.6, and 0%, respectively. This finding shows that the low difference between the results increases the accuracy of the analysis.

8 Theoretical validation

Theoretical approach was utilized to define the accuracy of CFD results. Heat transfer efficiency of NFs such as h, NTU, τ_w, and f were calculated theoretically. Eqs. (32)–(35) were used to calculate h, NTU, and f, whereas Eq. (29) was utilized for τ_w.

Nu number depending on the Pr number and heat flux can be described as follows [64]:

$$\overline{\mathrm{Nu}}_D = 0.023\mathrm{Re}^{0.8}\mathrm{Pr}^{0.4}. \tag{32}$$

Pr number can be solved as follows [64]:

$$\mathrm{Pr} = \frac{\mu C_p}{k}. \tag{33}$$

h obtained by considering the Nu number can be explained as follows [64]:

$$h = \frac{k\overline{\mathrm{Nu}}_D}{D}, \tag{34}$$

f can be calculated as follows [64]:

$$\frac{1}{\sqrt{f}} = -2\log\left(\frac{e/D_{\mathrm{Tube}}}{3.7} + \frac{2.51}{\mathrm{Re}\sqrt{f}}\right). \tag{35}$$

The results calculated with the theoretical approach are compared with the results obtained depending on CFD analysis and are presented in Table 11.

Table 11 shows that the differences for h, NTU, τ_w, and f are 0.7, 0.1, 0.2, and 0.3%, respectively. Thus, it was determined that the CFD analysis was performed with high accuracy.

9 Conclusion

In this numerical, theoretical, and statistical research, the impact of NP type, VF, and Re number in the heat transfer efficiency of NFs were analyzed. Heat transfer coefficient, NTU, wall shear stress, and friction factor were considered as the heat transfer efficiency of NFs. ANSYS Fluent software was employed to perform computational fluid dynamics analyses. The test sequences of the analyses were designed according to the Taguchi method and the L9 orthogonal array was utilized. NP type, VF, and Re number were considered as decisive factors. S/N ratio analysis was applied to determine the optimal levels of decisive factors on the heat transfer efficiency of NFs. Significance levels and contribution rates of the decisive factors on the heat transfer efficiency were evaluated utilizing Analysis of Variance. The important findings obtained from the numerical, statistical, and theoretical study are summarized. The most effective NPs on h and τ_w were identified as Gr, Al_2O_3, and Cu, respectively. For NTU, the most effective NPs are found to be Cu, Al_2O_3, Gr, respectively. However, no effect of NPs on f could be detected. The increasing Re number from 6,000 to 8,000 causes an increase in h and τ_w and a decrease in NTU and f. The increasing volume fractions of NPs from 0.5 to 1.5% causes an increase in h, NTU, and τ_w, but no effect was observed on f. The optimum h and τ_w data were obtained using 1.5%Gr NFs, and Re number of 8,000. However, the optimum NTU was achieved utilizing 1.5%Cu NFs and Re number of 6,000. According to ANOVA, Re number on h, NTU, and τ_w was detected as a significant decisive factor. The most effective decisive factors on h were achieved to be Re number with 98.58% impact, NP with 1.09% impact, and volume fraction with 0.26% impact, respectively. The most powerful decisive factors for NTU were obtained as Re number with 56.30% impact, NP with 28.04% impact, and volume fraction with 13.54% impact, respectively. The most dominant decisive factors on τ_w were considered as Re number with 97.88% impact, NP with 1.82% impact, and volume fraction with 0.14% impact, respectively. The differences for h, NTU, τ_w, and f were found to be 0.2, 1, 0.6, and 0% in statistical verification, whereas these differences were detected as 0.7, 0.1, 0.2, and 0.3% in theoretical verification.

Funding information: The author states no funding involved.

Author contribution: The author has accepted responsibility for the entire content of this manuscript and approved its submission.

Conflict of interest: The author states no conflict of interest.

Data availability statement: All data generated or analyzed during this study are included in this published article.

References

[1] Kalsi S, Kumar S, Kumar A, Alam T, Dobrotă D. Thermophysical properties of nanofluids and their potential applications in heat

transfer enhancement: A review. Arab J Chem. 2023;16:105272. doi: 10.1016/j.arabjc.2023.105272.
[2] Louis SP, Ushak S, Milian Y, Nemś M, Nemś A. Application of nanofluids in improving the performance of double-pipe heat exchangers—A critical review. Materials. 2022;15:6879.
[3] Rabby M, Hossain F, Amin S, Mumu TA, Bhuiyan M, Islam A. Convective heat transfer and power saving application of Si based nanoparticles in a circular pipe. Lat Am Appl Res. 2020;50:321–7.
[4] Tawalbeh M, Shomope I, Al-Othman A. Comprehensive review on non-Newtonian nanofluids, preparation, characterization, and applications. Int J Thermofluids. 2024;22:100705. doi: 10.1016/j.ijft.2024.100705.
[5] Rabby MII, Uddin MW, Hassan NMS, Al Nur M, Uddin R, Istiaque S, et al. Recent progresses in tri-hybrid nanofluids: A comprehensive review on preparation, stability, thermo-hydraulic properties, and applications. J Mol Liq. 2024;408:125257. doi: 10.1016/j.molliq.2024.125257.
[6] El hadoui B, Kaddiri M. Aspect ratio's critical role in enhancing natural convective heat transfer with temperature-dependent nanofluids within rectangular enclosures. Int J Thermofluids. 2023;20:100501. doi: 10.1016/j.ijft.2023.100501.
[7] Abdelaziz AH, El-Maghlany WM, Alaa El-Din A, Alnakeeb MA. Mixed convection heat transfer utilizing nanofluids, ionic nanofluids, and hybrid nanofluids in a horizontal tube. Alex Eng J. 2022;61:9495–508. doi: 10.1016/j.aej.2022.03.001.
[8] Ghazanfari V, Taheri A, Amini Y, Mansourzade F. Enhancing heat transfer in a heat exchanger: CFD study of twisted tube and nanofluid (Al_2O_3, Cu, CuO, and TiO_2) effects. Case Stud Therm Eng. 2024;53:103864. doi: 10.1016/j.csite.2023.103864.
[9] Xuan Z, Wang S, Zhai Y, Wang H. Thermodynamic performance of Al_2O_3-Cu-CuO/water (W) ternary nanofluids in the full-flow regime of convective heat transfer. Exp Therm Fluid Sci. 2023;147:110959. doi: 10.1016/j.expthermflusci.2023.110959.
[10] Amjadian M, Safarzadeh H, Bahiraei M, Nazari S, Jaberi B. Heat transfer characteristics of impinging jet on a hot surface with constant heat flux using Cu2O–water nanofluid: An experimental study. Int Commun Heat Mass Transf. 2020;112:104509. doi: 10.1016/j.icheatmasstransfer.2020.104509.
[11] Mukherjee S, Poloju V, Mishra PC. Heat transfer, exergoeconomic performance and sustainability impact of a novel CuO+ MgO+ GO/water ternary nanofluid. Appl Therm Eng. 2023;235:121391. doi: 10.1016/j.applthermaleng.2023.121391.
[12] Jain R, Mehta R, Bhatnagar A, Ahmad H, Khan ZA, Ismail GM. Numerical study of heat and mass transfer of williamson hybrid nanofluid (CuO/CNT's-water) past a permeable stretching/shrinking surface with mixed convective boundary condition. Case Stud Therm Eng. 2024;59:104313. doi: 10.1016/j.csite.2024.104313.
[13] Alklaibi A, Sundar LS, Mouli KVC. Experimental investigation on the performance of hybrid Fe_3O_4 coated MWCNT/water nanofluid as a coolant of a plate heat exchanger. Int J Therm Sci. 2022;171:107249.
[14] Rostami MH, Najafi G, Ghobadin B, Motevali A. Thermal performance investigation of SWCNT and graphene quantum dots nanofluids in a shell and tube heat exchanger by using fin blade tubes. Heat Transf. 2020;49:4783–800.
[15] Calviño U, Montenegro I, Sohel Murshed SM, Fernández-Seara J, Vallejo JP, Lugo L. Heat transfer and hydrodynamic performance of ZrO_2 geothermal nanofluids through tubular and plate heat exchangers. Appl Therm Eng. 2024;253:123770. doi: 10.1016/j.applthermaleng.2024.123770.
[16] Saini R, Gupta B, Prasad Shukla A, Singh B, Baredar P, Bisen A. CFD analysis of heat transfer enhancement in a concentric tube counter flow heat exchanger using nanofluids (SiO_2/H_2O, Al_2O_3/H_2O, CNTs/H_2O) and twisted tape turbulators. Mater Today: Proc. 2023;76:418–29. doi: 10.1016/j.matpr.2022.12.044.
[17] Karimi S, Heyhat MM, Isfahani AHM, Hosseinian A. Experimental investigation of convective heat transfer and pressure drop of SiC/water nanofluid in a shell and tube heat exchanger. Heat Mass Transf. 2020;56:2325–31.
[18] Behrozifard A, Goshayeshi HR, Zahmatkesh I, Chaer I, Salahshour S, Toghraie D. Experimental optimization of the performance of a plate heat exchanger with Graphene oxide/water and Al_2O_3/water nanofluids. Case Stud Therm Eng. 2024;59:104525. doi: 10.1016/j.csite.2024.104525.
[19] Evran S, Kurt M. CFD analysis of particle shape and Reynolds number on heat transfer characteristics of nanofluid in heated tube. Open Phys. 2024;22:20240046.
[20] Bisheh MM, Pourfallah M, Gholinia M. Impact of hybrid nanofluids (Ag-TiO_2/H_2O) on improving the performance of a heat exchanger with turbulent induction elements. Eng Rep. 2022;4:e12502.
[21] Saleh B, Sundar LS. Experimental study on heat transfer, friction factor, entropy and exergy efficiency analyses of a corrugated plate heat exchanger using Ni/water nanofluids. Int J Therm Sci. 2021;165:106935.
[22] Sridhar S, Karuppasamy R, Sivakumar G. Experimental investigation of heat transfer enhancement of shell and tube heat exchanger using SnO_2-water and Ag-water nanofluids. J Therm Sci Eng Appl. 2020;12:041016.
[23] Ziyadanogullari NB, Percin S. An experimental investigation of the effects of using hexagonal BN–water nanofluids on the thermal performance and pressure drop of a concentric tube heat exchanger. Energies. 2024;17:1269.
[24] Afridi MI, Srinivas Reddy C, Deepika AR, Govardhan K. Thermal analysis of AIN-Al2O3 Casson hybrid nano fluid flow through porous media with inclusion of slip impact. Case Stud Therm Eng. 2024;60:104783. doi: 10.1016/j.csite.2024.104783.
[25] Pattanayak B, Mund A, Jayakumar J, Parashar K, Parashar SK. Estimation of Nusselt number and effectiveness of double-pipe heat exchanger with Al_2O_3–, CuO–, TiO_2–, and ZnO–water based nanofluids. Heat Transf. 2020;49:2228–47.
[26] Bretado-de los Rios MS, Rivera-Solorio CI, Nigam KDP. An overview of sustainability of heat exchangers and solar thermal applications with nanofluids: A review. Renew Sustain Energy Rev. 2021;142:110855. doi: 10.1016/j.rser.2021.110855.
[27] Sreenivasulu Reddy G, Kalaivanan R, Uday Kumar R, Krishna Varma K. Augmenting heat transfer performance in a heat exchanger with CeO2 nanofluids. Mater Res Innov. 2024;28:19–31.
[28] Siddiqui OK, Shams A, Al-Athel K. A comprehensive review on the use of nanoparticles in nuclear power plants. Arab J Sci Eng. 2023;28:1–25.
[29] Ghalandari M, Maleki A, Haghighi A, Shadloo MS, Nazari MA, Tlili I. Applications of nanofluids containing carbon nanotubes in solar energy systems: A review. J Mol Liq. 2020;313:113476.
[30] Nobrega G, de Souza RR, Gonçalves IM, Moita AS, Ribeiro JE, Lima RA. Recent developments on the thermal properties, stability and applications of nanofluids in machining, solar energy and biomedicine. Appl Sci. 2022;12:1115.
[31] Pordanjani AH, Aghakhani S, Afrand M, Mahmoudi B, Mahian O, Wongwises S. An updated review on application of nanofluids in heat exchangers for saving energy. Energy Convers Manag. 2019;198:111886.

[32] Tyagi PK, Kumar R, Mondal PK. A review of the state-of-the-art nanofluid spray and jet impingement cooling. Phys Fluids. 2020;32(12):121301. doi: 10.1063/5.0033503.
[33] Chinchanikar S, Kore SS, Hujare P. A review on nanofluids in minimum quantity lubrication machining. J Manuf Process. 2021;68:56–70.
[34] Oliveira GA, Cardenas Contreras EM, Bandarra Filho EP. Experimental study of thermophysical properties of MWCNT and graphene coolant nanofluids for automotive application. J Braz Soc Mech Sci Eng. 2021;43:1–13.
[35] Bahiraei M, Heshmatian S. Electronics cooling with nanofluids: A critical review. Energy Convers Manag. 2018;172:438–56.
[36] Thianpong C, Wongcharee K, Kunnarak K, Chokphoemphun S, Chamoli S, Eiamsa-ard S. Parametric study on thermal performance augmentation of TiO_2/water nanofluids flowing a tube contained with dual counter twisted-tapes. Case Stud Therm Eng. 2024;59:104471. doi: 10.1016/j.csite.2024.104471.
[37] Muhammad Rizwan H, Ahmad Cheema T, Abdul Karim R, Mohib Ur Rehman M, Woo Park C. Experimental thermal performance intensification of gravitational water vortex heat exchanger using hexagonal boron Nitride-water nanofluid. Appl Therm Eng. 2024;254:123834. doi: 10.1016/j.applthermaleng.2024.123834.
[38] Afzal S, Qayyum M, Akgül A, Hassan AM. Heat transfer enhancement in engine oil based hybrid nanofluid through combustive engines: An entropy optimization approach. Case Stud Therm Eng. 2023;52:103803. doi: 10.1016/j.csite.2023.103803.
[39] Kiruba R, Kingson Solomon Jeevaraj A. Rheological characteristics and thermal studies of EG based Cu:ZnO hybrid nanofluids for enhanced heat transfer efficiency. Chem Phys Impact. 2023;7:100278. doi: 10.1016/j.chphi.2023.100278.
[40] Zhang L, Wang S, Qu P, Song J, Zhang H, Lu T, et al. Analysis of nanofluid flow and heat transfer characteristics in a wavy-walled tube heat exchanger. Int J Heat Fluid Flow. 2024;108:109488. doi: 10.1016/j.ijheatfluidflow.2024.109488.
[41] Fares M, Al-Mayyahi M, Al-Saad M. Heat transfer analysis of a shell and tube heat exchanger operated with graphene nanofluids. Case Stud Therm Eng. 2020;18:100584. doi: 10.1016/j.csite.2020.100584.
[42] Fule PJ, Bhanvase BA, Sonawane SH. Experimental investigation of heat transfer enhancement in helicalcoil heat exchangers using water based CuO nanofluid. Adv Powder Technol. 2017;28:2288–94. doi: 10.1016/j.apt.2017.06.010.
[43] Said Z, Rahman SMA, El Haj Assad M, Alami AH. Heat transfer enhancement and life cycle analysis of a shell-and-tube heat exchanger using stable CuO/water nanofluid. Sustain Energy Technol Assess. 2019;31:306–17. doi: 10.1016/j.seta.2018.12.020.
[44] Salameh T, Alkasrawi M, Olabi AG, Makky AA, Abdelkareem MA. Experimental and numerical analysis of heat transfer enhancement inside concentric counter flow tube heat exchanger using different nanofluids. Int J Thermofluids. 2023;20:100432. doi: 10.1016/j.ijft.2023.100432.
[45] Qi C, Luo T, Liu M, Fan F, Yan Y. Experimental study on the flow and heat transfer characteristics of nanofluids in double-tube heat exchangers based on thermal efficiency assessment. Energy Convers Manag. 2019;197:111877. doi: 10.1016/j.enconman.2019.111877.
[46] Ajeeb W, Thieleke da Silva RRS, Murshed SMS. Experimental investigation of heat transfer performance of Al_2O_3 nanofluids in a compact plate heat exchanger. Appl Therm Eng. 2023;218:119321. doi: 10.1016/j.applthermaleng.2022.119321.
[47] Zheng D, Wang J, Chen Z, Baleta J, Sundén B. Performance analysis of a plate heat exchanger using various nanofluids. Int J Heat Mass Transf. 2020;158:119993. doi: 10.1016/j.ijheatmasstransfer.2020.119993.
[48] Bahiraei M, Ahmadi AA. Thermohydraulic performance analysis of a spiral heat exchanger operated with water–alumina nanofluid: Effects of geometry and adding nanoparticles. Energy Convers Manag. 2018;170:62–72. doi: 10.1016/j.enconman.2018.05.061.
[49] Abro KA, Al-Mdallal QM, Memon IQ. Sinusoidal heating on convective heat transfer of nanofluid under differential technique. ZAMM - J Appl Math Mech/Zeitschrift für Angewandte Mathematik und Mechanik. 2024;104:e202300895. doi: 10.1002/zamm.202300895.
[50] Memon IQ, Abro KA, Solangi MA, Shaikh AA. Thermal optimization and magnetization of nanofluid under shape effects of nanoparticles. South Afr J Chem Eng. 2023;45:201–9. doi: 10.1016/j.sajce.2023.05.012.
[51] Riaz S, Amir M, Memon IQ, Ali Q, Abro KA. A comparative study for solidification of nanoparticles suspended in nanofluids through non-local kernel approach. Arab J Sci Eng. 2023;48:11645–63. doi: 10.1007/s13369-022-07493-y.
[52] Amir M, Ali Q, Abro KA, Raza A. Characterization nanoparticles via Newtonian heating for fractionalized hybrid nanofluid in a channel flow. J Nanofluids. 2023;12:987–95. doi: 10.1166/jon.2023.1982.
[53] ANSYS. Fluent software material database. Canonsburg, PA: ANSYS Inc; 2021.
[54] Dalkılıç AS, Mercan H, Özçelik G, Wongwises S. Optimization of the finned double-pipe heat exchanger using nanofluids as working fluids. J Therm Anal Calorim. 2021;143:859–78. doi: 10.1007/s10973-020-09290-x.
[55] Khanafer K, Vafai K. A critical synthesis of thermophysical characteristics of nanofluids. Int J Heat Mass Transf. 2011;54:4410–28. doi: 10.1016/j.ijheatmasstransfer.2011.04.048.
[56] Pak BC, Cho YI. Hydrodynamic and heat transfer study of dispersed fluids with submicron metallic oxide particles. Exp Heat Transf. 1998;11:151–70. doi: 10.1080/08916159808946559.
[57] Xuan Y, Roetzel W. Conceptions for heat transfer correlation of nanofluids. Int J Heat Mass Transf. 2000;43:3701–7.
[58] Maxwell JC. A treatise on electricity and magnetism. 3rd edn. Oxford U.K.: Clarendon Press; 1891.
[59] Leong KC, Yang C, Murshed SMS. A model for the thermal conductivity of nanofluids – the effect of interfacial layer. J Nanopart Res. 2006;8:245–54. doi: 10.1007/s11051-005-9018-9.
[60] Brinkman HC. The viscosity of concentrated suspensions and solutions. J Chem Phys. 1952;20:571.
[61] Ahsan M. Numerical analysis of friction factor for a fully developed turbulent flow using k–ε turbulence model with enhanced wall treatment. Beni-Suef Univ J Basic Appl Sci. 2014;3:269–77. doi: 10.1016/j.bjbas.2014.12.001.
[62] ANSYS. Ansys Fluent 12.0 theory guide. Canonsburg, PA: ANSYS Inc; 2009.
[63] Ross PJ. Taguchi techniques for quality engineering. 2nd edn. New York, USA: McGraw-Hill International Editions; 1996.
[64] Cengel Y. Heat transfer: A practical approach. 2nd edn. New York: McGraw-Hill; 2002.
[65] Garud KS, Lee M-Y. Numerical investigations on heat transfer characteristics of single particle and hybrid nanofluids in uniformly heated tube. Symmetry. 2021;13:876.